



Article

An Approach to Predicting the Ballistic Limit of Thin Textile-Reinforced Concrete Plates Based on Experimental Results

Marcus Hering ¹, Jürgen Sievers ², Manfred Curbach ³ and Birgit Beckmann ^{3,*}

¹ Bundesanstalt für Materialforschung und -Prüfung (BAM), Unter den Eichen 87, 12205 Berlin, Germany; marcus.hering@bam.de

² Gesellschaft für Anlagen- und Reaktorsicherheit (GRS) gGmbH, Schwertnergasse 1, 50667 Köln, Germany; juergen.sievers@grs.de

³ Institute of Concrete Structures, Technische Universität Dresden, 01062 Dresden, Germany; manfred.curbach@tu-dresden.de

* Correspondence: birgit.beckmann@tu-dresden.de

Abstract: In this article, a partial selection of experiments on enhancing the impact resistance of structural components with non-metallic, textile-reinforced concrete is discussed. The focus is on the experimental investigations in which the impact resistance of thin, textile-reinforced concrete plates is characterized. The article discusses the materials, fabrics and test setup used. For the experimental work, a drop tower from the Otto Mohr Laboratory, which belongs to the Technische Universität Dresden, was used. Furthermore, the experimental results are presented and evaluated using different methods. Based on the collected data, a suitable approach to determining the perforation velocity of an impactor through the investigated thin, textile-reinforced concrete plates is shown.

Keywords: accelerated drop tower tests; perforation limit; experimental investigation; impact load; textile-reinforced concrete; non-metallic reinforcement; strengthening; sustainability



Citation: Hering, M.; Sievers, J.; Curbach, M.; Beckmann, B. An Approach to Predicting the Ballistic Limit of Thin Textile-Reinforced Concrete Plates Based on Experimental Results. *Buildings* **2023**, *13*, 2234. <https://doi.org/10.3390/buildings13092234>

Academic Editor: Flavio Stochino

Received: 2 August 2023

Revised: 24 August 2023

Accepted: 29 August 2023

Published: 2 September 2023



Copyright: © 2023 by the authors. Licensee MDPI, Basel, Switzerland. This article is an open access article distributed under the terms and conditions of the Creative Commons Attribution (CC BY) license (<https://creativecommons.org/licenses/by/4.0/>).

1. Introduction

1.1. Overview of the Research Objective

The design of structures against unusual load situations such as vehicular impact, aircraft crash or explosion is conducted on the basis of design codes or complex numerical simulations in order to determine the complex processes, and to be able to describe them at a component level. These load situations can be taken into account when planning new buildings. However, the problem arises when dealing with existing structures where, for a variety of reasons, the consideration of such extraordinary load situations subsequently becomes relevant. Reasons for this include newly created hazardous situations of particularly exposed buildings or a change in the use of existing buildings. Therefore, the question arises whether an existing building has to be demolished and replaced or whether it is possible to subsequently strengthen such a building for new load cases.

Within the framework of the Research Training Group 2250 (GRK2250)'s "Mineral-bonded composites for enhanced structural impact safety", funded by the German Research Foundation (DFG), this question is being examined in detail. This paper is focused on strengthening the layers of fine-grained concrete with non-metallic reinforcements that are applied on the rear side of the impacted structure.

These thin, strengthening layers were the focus of the investigations, as they form an essential part of the overall strengthening concept. This consists, on the one hand, of the reinforced concrete plate to be strengthened and, on the other hand, of the aforementioned strengthening layer. Since the combined load-bearing behavior of the reinforced concrete plate and the strengthening layer is extremely complex, it was decided that the two parts of

the system would be considered separately from each other at first. One part of the study of the reinforcing layer is the core topic of this paper. This is the perforation resistance of the strengthening layer. Another point of investigation that was considered is the bending behavior of the strengthening layer. However, this was carried out as a comprehensive analysis in the context of strengthened reinforced concrete plates. These investigations are not part of this article, but please see Hering [1] for more information.

1.2. State of the Art

An essential question for the rear-side strengthening of structures or components is the material to be used for the strengthening layer. A wide range of materials and material combinations is available for this purpose. One of the most important factors for such a strengthening layer is that it is as thin and effective as possible, and saves unnecessary dead load. For instance, ultra-high-performance fiber-reinforced concrete (UHPFRC) was proven to increase resistance to a high velocity small projectile impact [2,3] as the damage is highly localized. For larger projectile diameters, UHPFRC is not so effective as the fibers cannot prevent the separation of the punching cone. In contrast to the short fibers, the membrane action of textile-reinforced concrete can be utilized for this type of projectile. In addition, textile-reinforced concrete satisfies all of the above-mentioned requirements and can be applied to existing concrete structures easily. Textile-reinforced concrete is a strengthening material or layer that is made of concrete or fine concrete (matrix material) and a fabric that is embedded in this layer. Especially in the case of carbon fabrics, the term carbon-reinforced concrete is used. If a different material or combination of materials is used, it is more commonly called textile-reinforced concrete. A variety of different fabric configurations, e.g., uniaxial, biaxial, or multiaxial, can be used as the reinforcement structure. In the case of static loading, the selection criteria for the reinforcement structure are clearly defined. Carbon-reinforced concrete in particular has already proven to be very effective at strengthening structural components to increase the load-bearing capacity for static loads; see [4–6]. In the case of impact loads, however, the selection criteria cannot be defined so clearly, as the loads applied to a component cannot be classified as clearly as in the case of static loads. The impact loading results in a significant localization of damage and a mixture of punching and bending failure, as presented in Hering and Curbach [7] and Hering et al. [8]. The evaluation of a large test program to determine the efficiency of different textile-reinforced concrete configurations was carried out in Hering [1]. Based on the data published in these publications, a new interpretation of the test data and a comparison with the approach presented in Hering [1] follows. This is accompanied by a simplified approach to determining the ballistic limit of small-scale plates under examination.

Ballistic limit, or perforation velocity, is the velocity at which a projectile starts to perforate a material or structure. It should be noted that the ballistic limit value only applies to the combination of a projectile and a target structure. Important parameters of the projectile are its shape and material. On the side of the target structure, the material and thickness, as well as the inner structure of the target, are significant. Usually, the ballistic limit is determined experimentally. For this purpose, the target structure is shot with projectiles. The velocity of the projectiles is increased until the ballistic limit is found. A large number of tests are necessary to statistically validate this value. In this context, the ballistic limit or the perforation velocity is often given as v_{50} . This term refers to the projectile velocity at which 50% of the projectiles get stuck in the target structure and 50% perforate it. Studies in this area include Tahenti et al. [9], Johnson et al. [10] and Keubuehl [11].

2. Materials and Methods

2.1. Fine Concrete

The applied matrix material is a fine concrete that is already used for static strengthening applications. It is the product PAGEL®/TUDALIT®-FEINBETON (Pagel TF10 in short). Pagel TF10 is a ready-made dry mix product to which only water needs to be added (3.5 l per 25 kg dry mixture, [12]). The maximum grain size of the fine concrete is 1 mm. A fine concrete compressive strength of 95.7 N/mm² was determined using cubes with an edge length of 40 mm and an age of 56 days. For this purpose, a bending tensile/compressive strength test was carried out according to DIN EN 196-1 [13]. Furthermore, the bending tensile strength was determined to be 6.88 N/mm², and the density to be 2.15 g/cm³; see Hering [1].

2.2. Fabrics

The experiments considered in this article represent a selection from the complete set of experiments conducted. The compilation of all experimental data can be found in Hering [1]. The fabrics that were used are shown in Figure 1. There are three carbon fabrics (#1, #3 and #4) with different mesh sizes, and one glass fabric (#2). The fabrics also differ in the chemical composition of their impregnations. Fabric #1 has a styrene-butadiene rubber (SBR) impregnation, while there is no information on fabric #2 according to the datasheet [14]. Fabrics #3 and #4 are impregnated with epoxy resin (EP). However, the resulting differences in the composite behavior will not be discussed in more detail. For more information, please refer to Lorenz [15], Schütze et al. [16] and Schütze and Curbach [17].

The technical characteristics of the fabrics are summarized in Table 1. Based on these different fabric parameters, significant differences in the result values are to be expected.

Table 1. Technical characteristics of the fabrics.

	Label	Material	Impregnation	Mesh Size (mm)	Warp Thread (tex)	Weft Thread (tex)	Youngs-Modulus Warp Weft (GPa)	Tensile Strength Warp Weft (GPa)
#1	BZT1-TUDALIT **	carbon	SBR	11 × 14	3300	800	170 152 **	1.98 2.94 **
#2	SSA1363 ***	E-Glas	n.a.	4 × 5	640	320	n.a.	n.a.
#3	Solidian GRID Q142/142-CCE-38 *	carbon	EP	38 × 38	6400	6400	>180 >180 ****	2.50 2.80 ****
#4	Solidian GRID Q85/85-CCE-21 *	carbon	EP	21 × 21	3200	3200	>220 >205 *****	3.30 3.55 *****

* according to Cherif et al. [18]. ** according to DIBt [19]. *** according to Valmieras stikla škiedra [14], there is no impregnation for this reinforcement; Young's Modulus and tensile strength are not available (n.a.) for this reinforcement. **** Solidian GRID Q142/142-CCE-38 [20]. ***** Solidian GRID Q85/85-CCE-21 [21].

2.3. Specimens Used

Thin plates with a dimension of 610 mm × 610 mm × 30 mm were investigated in the experimental campaign. The plate and the support frame are shown as a cross-sectional drawing in Figure 2, and the manufacturing process is shown in Figure 3. Furthermore, a detailed drawing and photo of the impactor can be seen in Figure 4. During the casting of the plates (Figure 3), the formwork was half-filled with concrete and the textile reinforcement layers (fabric layers) were placed in the center of each of the specimens. Afterwards, the formwork was filled completely with concrete and the concrete was levelled.

Table 2 shows a compilation of the number of layers used for each of the fabrics. Furthermore, the reinforcement area per meter (a_{tex} (mm²/m)) resulting from the number of fabric layers was specified. The fabrics where two layers were used are uniaxial fabrics. This implies that there is a main bearing direction and an auxiliary bearing direction. For this reason, the two fabric layers used were applied at 90° to each other so that the plate was reinforced nearly identically in both directions. This was not necessary for fabrics #3 and #4, as these are already fabrics with the same reinforcement content in both directions.

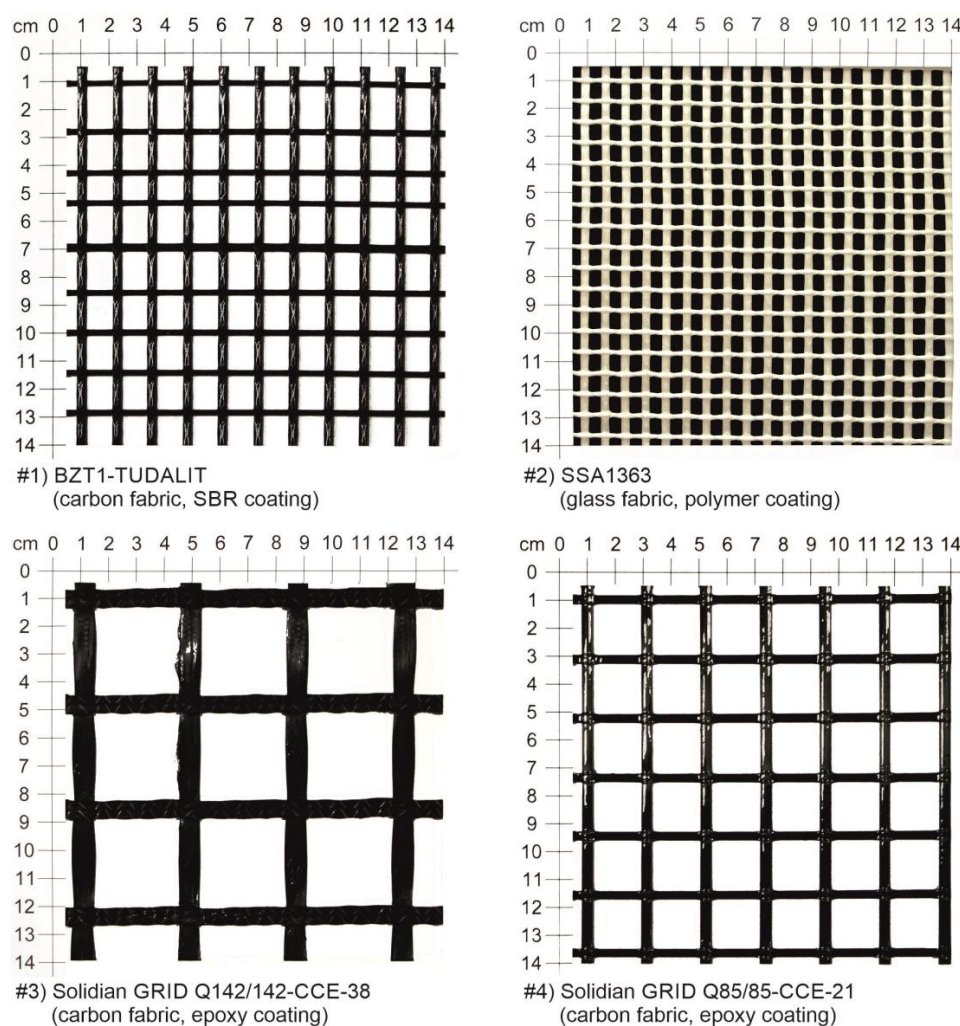


Figure 1. Selection of textile reinforcement fabrics; images: M. Hering.

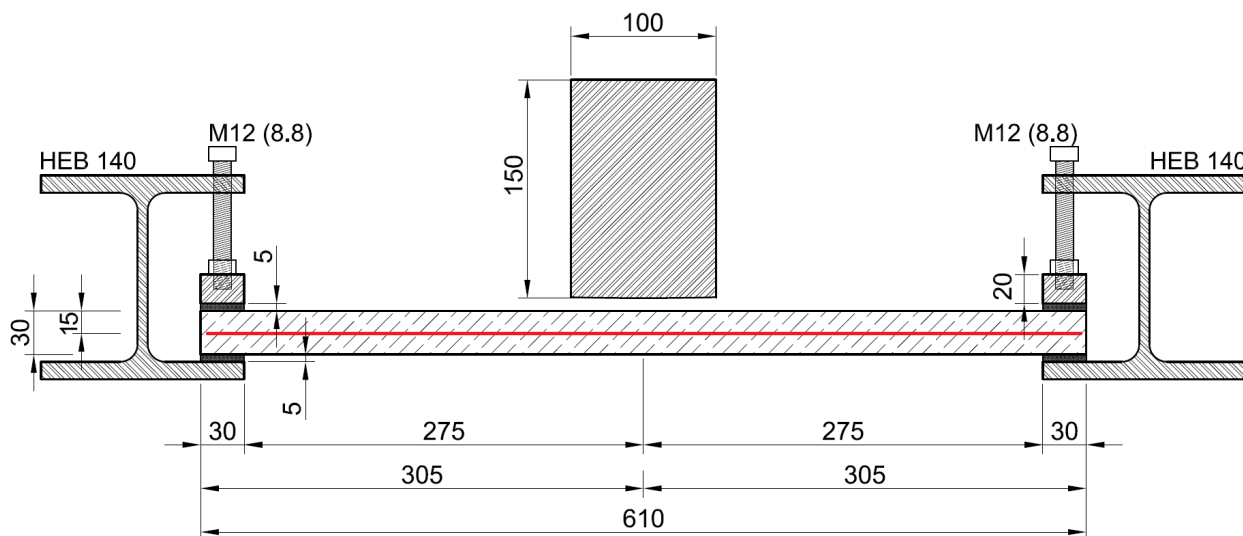


Figure 2. Specimen, support frame and impactor, according to Hering [1].

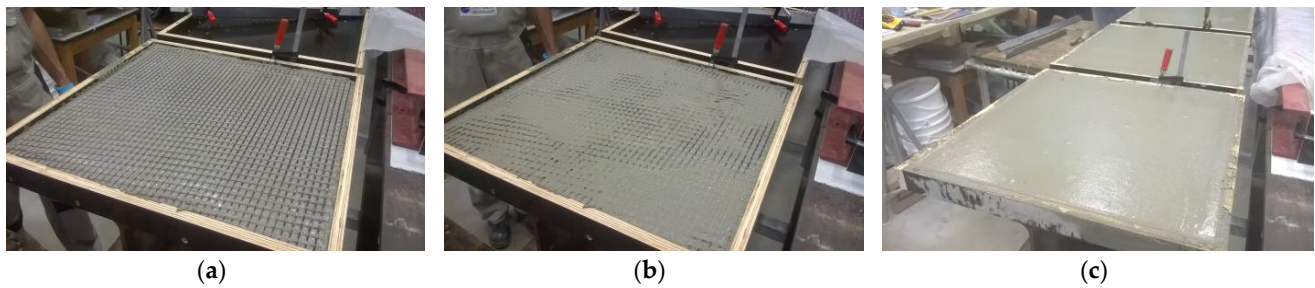


Figure 3. Manufacturing of test specimens. (a) Fabric embedded in fine concrete (15 mm thickness), (b) fabric pressed into fine concrete, and (c) test specimen filled with fine concrete (15 mm thickness) and smoothed (Hering [1]).

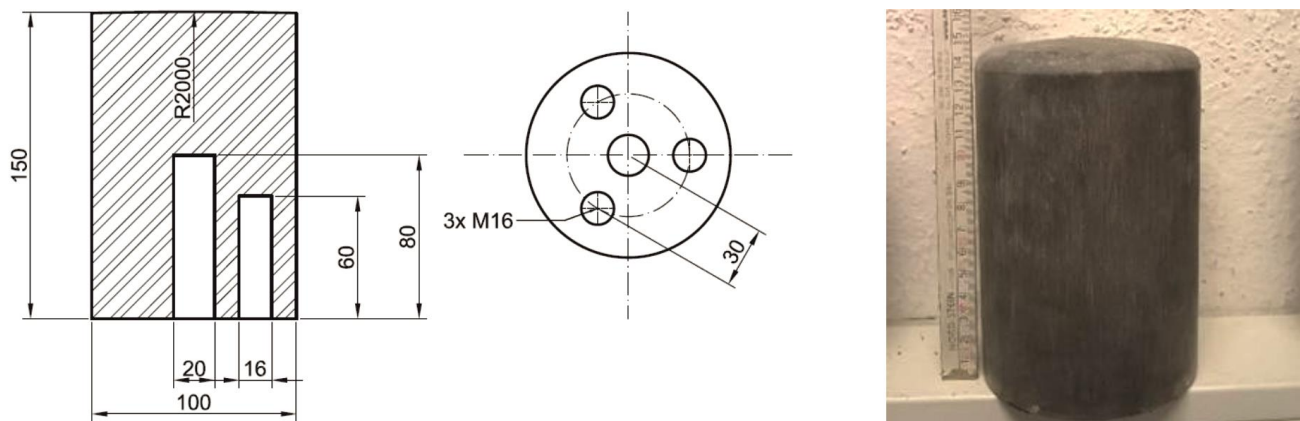


Figure 4. Detailed drawing of the impactor according to [7] and photo of the impactor (Hering [1]).

Table 2. Overview of the fabric, reinforcement area and number of test specimens.

Fabric	Number of Layers	a_{tex} (mm ² /m)	Number of Tested Specimens
Plain concrete (pc)	/	0.00	10
#1	2	173.39 + 31.19	15
#2	2	54.48 + 22.7	9
#3	1	142	17
#4	1	85	16

To better understand the effect of the fabrics, unreinforced plates were also fabricated and tested. The experimental overview is presented in Table 2. This is an extraction of the entire test program, which can be found in its complete form in Hering [1].

2.4. Experimental Setup and Measurement System

The experimental setup used is shown in Figure 5. It is described in more detail in Hering et al. [7,8] and Hering [1]. Figure 5b shows the support frame in which the test specimen (small-scale plate) was clamped. Figure 2 shows the cross-section of the support frame. Using the screws shown in Figures 2 and 5, the plate was clamped with the help of a torque screwdriver to the same torque level to ensure repeatable boundary conditions. To fix the specimens, additional 5 mm-thick rubber strips were used; see Figure 2. These were primarily used to compensate for possible surface irregularities of the specimens and to apply the clamping force equally to the specimens.

Figure 5a shows the stereo high-speed camera system (SHSKS) that was used for the main data measurement.

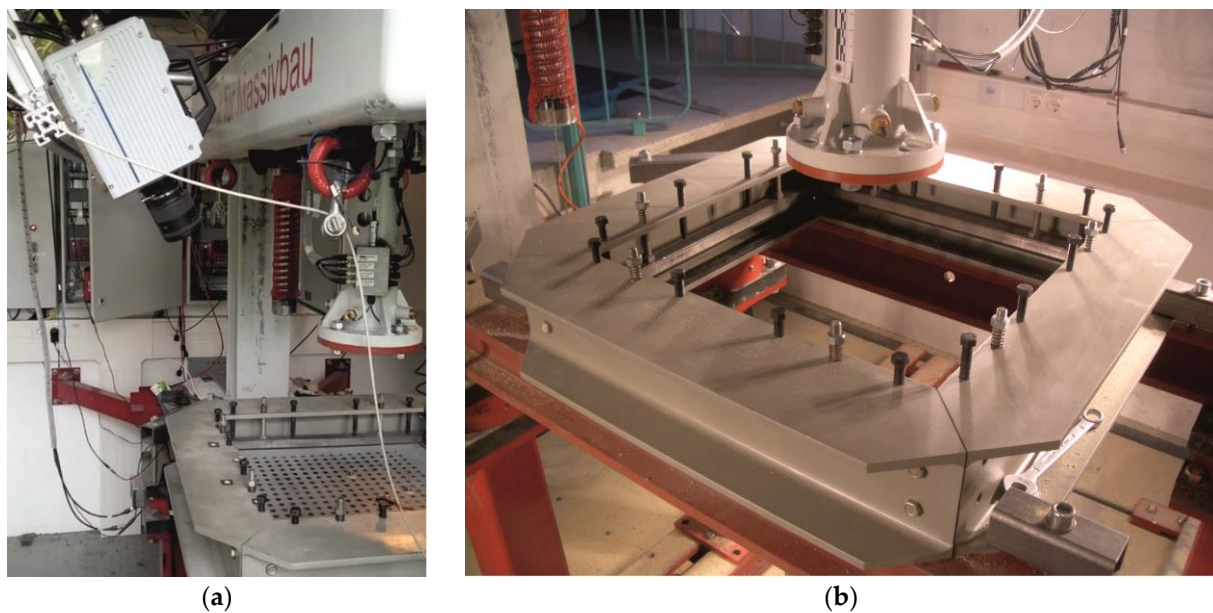


Figure 5. (a) Specimen mounted in the drop-tower before an experiment, and (b) support frame (Hering [1]).

The resolution of the two cameras integrated in the SHSKS was $1024 \text{ px} \times 1024 \text{ px}$ each. The recording speed was 5000 fps (frames per second). The image data were evaluated using the 3D photogrammetric digital image correlation and analysis software Aramis from the company GOM.

The impact load was applied using the accelerated modification of the drop tower facility located in the Otto Mohr Laboratory at the Technische Universität Dresden. A detailed description of this facility can be found in Just et al. [22] and Hering et al. [23].

A cylindrical steel impactor/projectile with a diameter of 100 mm, a length of 150 mm and a weight (m_{Imp}) of 8.4 kg was used. The experimental setup including the test specimens, supporting frame and impactor is shown schematically in Figure 2. The nose of the impactor was slightly curved with a radius of 2000 mm. The impactor was accelerated in an 11 m-long acceleration tube with compressed air. The velocity of the impactor was recorded with the SHSKS during the entire time range relevant to the experiment. This was possible because the impactor was in free flight, i.e., outside the acceleration tube, immediately before hitting the test specimen. This free-flight phase allowed for a view of the rear of the impactor, as well as for the photogrammetric velocity evaluation.

3. Results and Evaluation

3.1. Experimental Results

The evaluation of the experiments was based on the velocity of the impactor. By using 3D photogrammetry, the velocity of the impactor was measured during the entire process of impact, deceleration and perforation. The focus of the experimental evaluation in this publication is the consideration of the velocity of the impactor immediately before it hits the specimen (v_1) and the velocity of the impactor after it has perforated the specimen (v_2). When the impactor became stuck in the specimen, the velocity (v_2) was 0.00 m/s. When it rebounded, the velocity (v_2) could also be determined using photogrammetry and was given a negative sign. Furthermore, it was considered whether the impactor perforated through the small-scale plate or not; see Tables 3–5.

Table 3. Overview of the test results of the plain fine concrete reference plates.

	Label Acc. to [1]	v_1 (m/s)	v_2 (m/s)	Δv (m/s)	$E_{kin,1}$ (J)	$E_{kin,2}$ (J)	ΔE_{kin} (J)	Perforation
pc-1	BP144	12.15	9.18	2.97	620.01	353.94	266.07	yes
pc-2	BP139	12.31	9.18	3.13	636.45	353.94	282.51	yes
pc-3	BP217	16.53	13.12	3.41	1147.61	722.96	424.65	yes
pc-4	BP140	19.68	15.65	4.03	1626.67	1028.67	598.00	yes
pc-5	BP065	20.30	16.54	3.76	1730.78	1149.00	581.78	yes
pc-6	BP066	24.71	20.84	3.87	2564.45	1824.08	740.37	yes
pc-7	BP218	25.17	21.28	3.89	2660.82	1901.92	758.90	yes
pc-8	BP141	27.95	23.07	4.88	3281.05	2235.34	1045.71	yes
pc-9	BP142	33.56	27.88	5.68	4730.35	3264.64	1465.71	yes
pc-10	BP143	43.60	37.92	5.68	7984.03	6039.29	1944.74	yes

Table 4. Overview of the test results of the test specimens with fabric #1.

	Label Acc. to [1]	v_1 (m/s)	v_2 (m/s)	Δv (m/s)	$E_{kin,1}$ (J)	$E_{kin,2}$ (J)	ΔE_{kin} (J)	Perforation
#1-1	BP129	9.83	−4.27	14.10	405.84	76.58	329.26	no
#1-2	BP153	15.38	−4.76	20.14	993.49	95.16	898.33	no
#1-3	BP133	17.95	−1.63	19.58	1353.25	11.16	1342.09	no
#1-4	BP130	20.03	0.00	20.03	1685.04	0.00	1685.04	no
#1-5	BP127	20.18	0.00	20.18	1710.38	0.00	1710.38	no
#1-6	BP154	20.25	0.00	20.25	1722.26	0.00	1722.26	no
#1-7	BP151	20.93	7.39	13.54	1839.87	229.37	1610.50	yes
#1-8	BP132	27.14	14.02	13.12	3093.63	825.55	2268.08	yes
#1-9	BP155	27.70	17.45	10.25	3222.62	1278.91	1943.71	yes
#1-10	BP134	28.44	15.10	13.34	3397.10	957.64	2439.46	yes
#1-11	BP152	28.77	16.58	12.19	3476.39	1154.56	2321.83	yes
#1-12	BP128	29.92	18.28	11.64	3759.87	1403.47	2356.40	yes
#1-13	BP135	32.79	21.38	11.41	4515.77	1919.84	2595.93	yes
#1-14	BP156	33.94	24.07	9.87	4838.08	2433.33	2404.75	yes
#1-15	BP131	34.53	23.41	11.12	5007.75	2301.72	2706.03	yes

In the case of perforation, punching failure occurred as the failure mode of the plate. Furthermore, cracks induced by bending could be seen on the side of the component facing away from the impact; see Figure 6c,d. In the case of the fully perforated specimens, it could be seen that the fabrics were ruptured in the area of the perforation. Whether the failure of the fabric was a pure tensile failure, or a combination of tensile and shear action, could not be clearly determined.

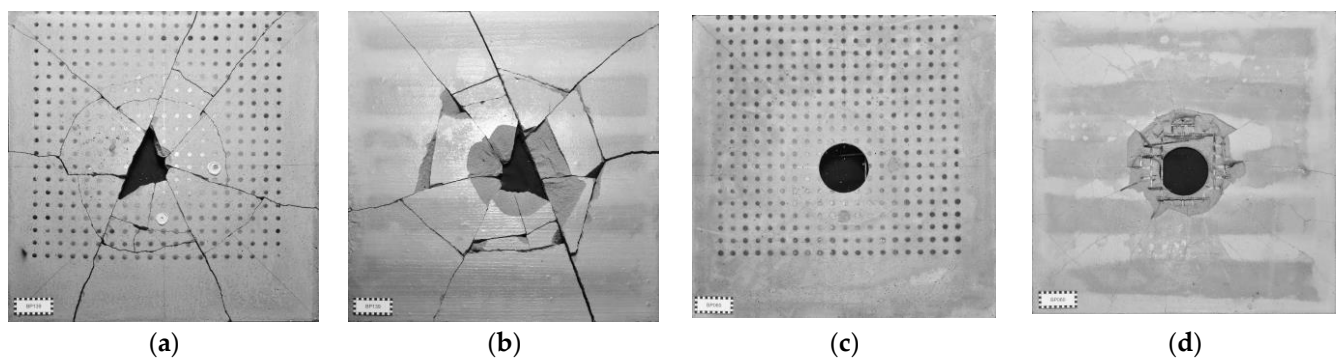
**Figure 6.** Examples of perforated specimens pc-2 (a) front side, and (b) back side; and #4-15 (c) front side, and (d) back side (Hering [1]).

Table 5. Overview of the test results of the test specimens with fabric #2, #3 and #4.

	Label Acc. to [1]	v_1 (m/s)	v_2 (m/s)	Δv (m/s)	$E_{kin,1}$ (J)	$E_{kin,2}$ (J)	ΔE_{kin} (J)	Perforation
#2-1	BP020	20.78	0.00	20.78	1813.60	0.00	1813.60	no
#2-2	BP019	21.07	0.00	21.07	1864.57	0.00	1864.57	no
#2-3	BP021	28.17	17.85	10.32	3332.91	1338.21	1994.70	yes
#2-4	BP229	28.17	17.51	10.66	3332.91	1287.72	2045.19	yes
#2-5	BP022	29.85	19.28	10.57	3742.29	1561.22	2181.07	yes
#2-6	BP230	31.03	23.50	7.53	4044.02	2319.45	1724.57	yes
#2-7	BP023	33.83	24.81	9.02	4806.77	2585.25	2221.52	yes
#2-8	BP231	34.29	26.98	7.31	4938.38	3057.27	1881.11	yes
#2-9	BP024	34.92	24.37	10.55	5121.51	2494.37	2627.14	yes
#3-1	BP031	11.19	−3.28	14.47	525.91	45.19	480.72	no
#3-2	BP041	14.78	6.07	8.71	917.48	154.75	762.73	yes
#3-3	BP029	15.29	4.06	11.23	981.89	69.23	912.66	yes
#3-4	BP042	19.58	11.44	8.14	1610.18	549.67	1060.51	yes
#3-5	BP032	20.30	12.37	7.93	1730.78	642.67	1088.11	yes
#3-6	BP025	20.32	10.29	10.03	1734.19	444.71	1289.48	yes
#3-7	BP026	20.54	13.43	7.11	1771.94	757.53	1014.41	yes
#3-8	BP033	23.70	16.76	6.94	2359.10	1179.77	1179.33	yes
#3-9	BP028	26.14	19.38	6.76	2869.86	1577.45	1292.41	yes
#3-10	BP039	27.02	21.04	5.98	3066.34	1859.26	1207.08	yes
#3-11	BP034	28.05	21.16	6.89	3304.57	1880.53	1424.04	yes
#3-12	BP027	28.06	20.60	7.46	3306.93	1782.31	1524.62	yes
#3-13	BP035	29.36	23.11	6.25	3620.44	2243.10	1377.34	yes
#3-14	BP038	31.59	25.39	6.20	4191.30	2707.54	1483.76	yes
#3-15	BP037	33.02	26.72	6.30	4579.35	2998.63	1580.72	yes
#3-16	BP030	33.94	27.00	6.94	4838.08	3061.80	1776.28	yes
#3-17	BP036	34.29	27.00	7.29	4938.38	3061.80	1876.58	yes
#4-1	BP052	11.22	−4.69	15.91	528.73	92.38	436.35	no
#4-2	BP055	13.02	0.00	13.02	711.99	0.00	711.99	no
#4-3	BP053	13.20	1.98	11.22	731.81	16.47	715.34	yes
#4-4	BP049	15.94	6.30	9.64	1067.15	166.70	900.45	yes
#4-5	BP061	17.29	8.32	8.97	1255.57	290.73	964.84	yes
#4-6	BP056	17.39	5.68	11.71	1270.13	135.50	1134.63	yes
#4-7	BP062	19.61	13.21	6.40	1615.12	732.92	882.20	yes
#4-8	BP057	19.80	12.90	6.90	1646.57	698.92	947.65	yes
#4-9	BP051	20.02	12.72	7.30	1683.36	679.55	1003.81	yes
#4-10	BP063	20.67	12.68	7.99	1794.45	675.29	1119.16	yes
#4-11	BP054	20.72	13.91	6.81	1803.14	812.65	990.49	yes
#4-12	BP058	22.77	15.98	6.79	2177.59	1072.51	1105.08	yes
#4-13	BP059	23.28	17.88	5.40	2276.23	1342.72	933.51	yes
#4-14	BP064	23.46	17.06	6.40	2311.56	1222.38	1089.18	yes
#4-15	BP060	25.96	20.43	5.53	2830.47	1753.02	1077.45	yes
#4-16	BP050	27.34	21.61	5.73	3139.40	1961.37	1178.03	yes

The reinforcing effect of the clutch can be seen well in Figure 6. While in pc-2 (Figure 6a,b) the plate breaks into many parts, in #4-15 (Figure 6c,d) it remains as a unit. This is due to the fact that the fabric bears the tensile forces that the unreinforced fine concrete cannot bear.

3.2. Experimental Evaluation Based on a Power Function

The first step of the evaluation of the experimental results deals with the determination of the impactor's difference in kinetic energy before the impact on the test specimen ($E_{kin,1}$) and after the perforation or rebound of the impactor ($E_{kin,2}$). The kinetic energy of the

impactor is determined according to Equation (1). Based on this, the energy difference is calculated according to Equation (2).

$$E_{kin,i} = \frac{1}{2} \cdot v^2 \quad i = 1, 2 \quad (1)$$

$$\Delta E_{kin} = E_{kin,1} - E_{kin,2} \quad (2)$$

The values of the kinetic energy differences (ΔE_{kin}) resulting from this calculation are plotted in Figure 7 against the kinetic energy of the impactor before the impact on the specimen ($E_{kin,1}$). From the experimental data, it can be seen that the higher the impact energy ($E_{kin,1}$) of the impactor, the higher the value of the energy difference (ΔE). However, it can also be stated on the basis of the compiled experimental results that this only has a sampling character. A much larger number of experiments is necessary to clearly identify the scattering that also occurs. For this reason, a functional relationship was created using the fit function described in Equation (3) with the parameters a and p . The considerations that led from a linear functional approach to the power function described in Equation (3) can be found in Hering [1].

$$\Delta E_{kin}(E_{kin,1}) = a \cdot (E_{kin,1})^p \quad (3)$$

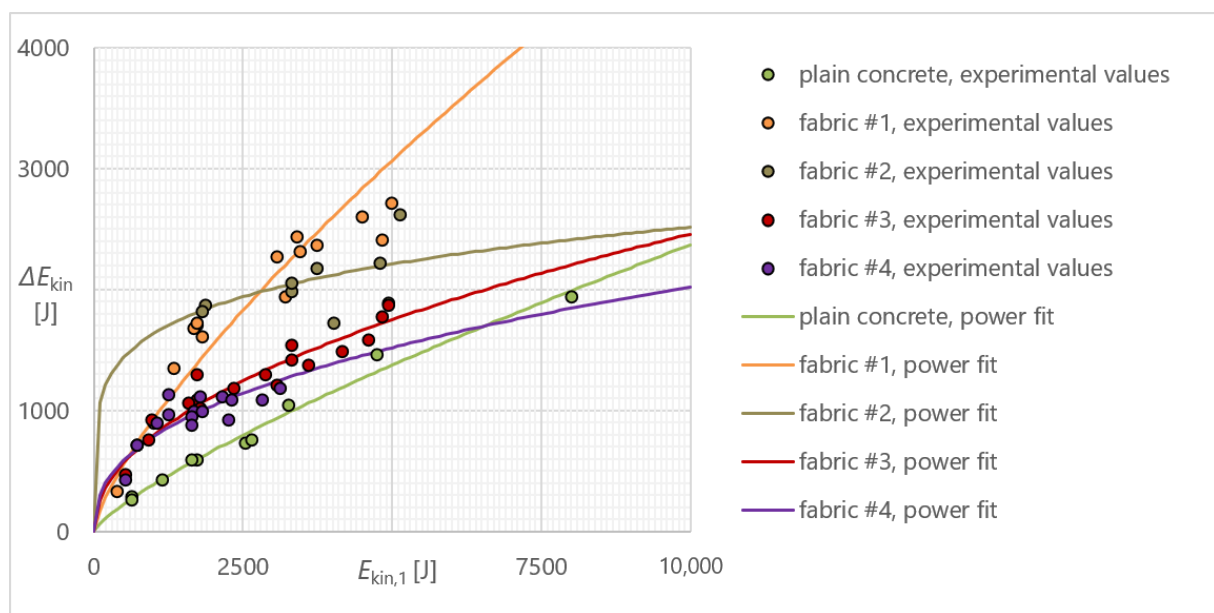


Figure 7. Visualization of the experimental results ΔE via $E_{kin,1}$ and fit according to Equation (3).

This was already carried out using the experimental data in Hering [1]. By choosing these fit functions, it is possible to show that an impact energy $E_{kin,1} = 0$ J also results in an energy difference $\Delta E = 0$ J. Furthermore, the power function can reproduce the experimental results well for higher energy ranges.

The fit parameters a and r , determined from the experimental data, as well as the coefficient of determination R^2 , are shown in Table 6. The visualization of the experimental data in Figure 7 shows an acceptable agreement with the selected fit using the determined parameters.

Using this method, it is possible to compare the impact resistance of the differently textile-reinforced concretes relative to each other, which was already carried out in Hering [1]. However, no further statements can be derived from this method. Only qualitative descriptions are possible. This evaluation of the test results also does not take into account the respective failure mode of the small-scale plates as a result of the impact event. However, it can be seen that the fine mesh reinforcement structures #1 and #2 increased the

values for ΔE significantly more than the large mesh reinforcement structures #3 and #4. As expected, the specimens without reinforcement structures showed the lowest values of ΔE .

Table 6. Fit parameters a and p and coefficient of determination R^2 for Equation (3) based on the experimental data.

Reinforcement Configuration	a (-)	p (-)	R^2 (-)
plain concrete	1.695	0.7864	0.9847
#1	5.390	0.7448	0.8921
#2	447.890	0.1874	0.2809
#3	26.815	0.4906	0.9062
#4	45.241	0.4126	0.6755

3.3. Experimental Evaluation Based on a Bilinear Functional Approach

Based on the conclusions of the previous section, a further evaluation method was developed with the help of the experimental results, which takes into account the different failure modes during the evaluation.

For this purpose, the experimental results were first plotted again in a diagram (see Figure 8). The values determined for ΔE were again mapped over $E_{kin,1}$. It can be seen that all data pairs of the values of “no perforation” are on a straight line with a slope of $m = 1.0$. In these experiments, it was found that the impactor either rebounds from the specimen or gets stuck in it. A significant decrease in the measured kinetic energy difference (ΔE) of the impactor can be observed only when it perforates through the specimen.

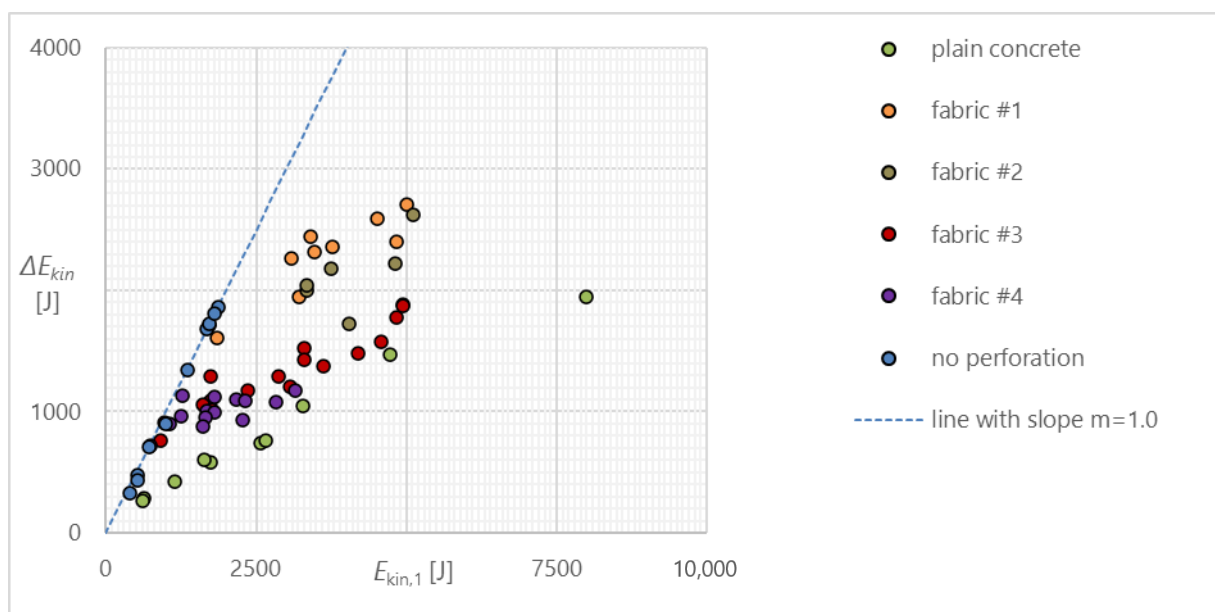


Figure 8. Visualization of the experimental results, with consideration of reinforcement and failure mode.

In Figure 9, a linear fit, according to Equation (4), is applied through the experimental data on the individual reinforcement configurations where a perforation of the impactor through the plate occurred. It can be seen that the linear fit follows the trend of the experimentally determined values very well. The values of the parameters m and n of Equation (4), resulting from the experimental values and the linear fit approach, are shown in Figure 9 and Table 7.

$$\Delta E_{kin}(E_{kin,1}) = m \cdot E_{kin,1} + n \quad (4)$$

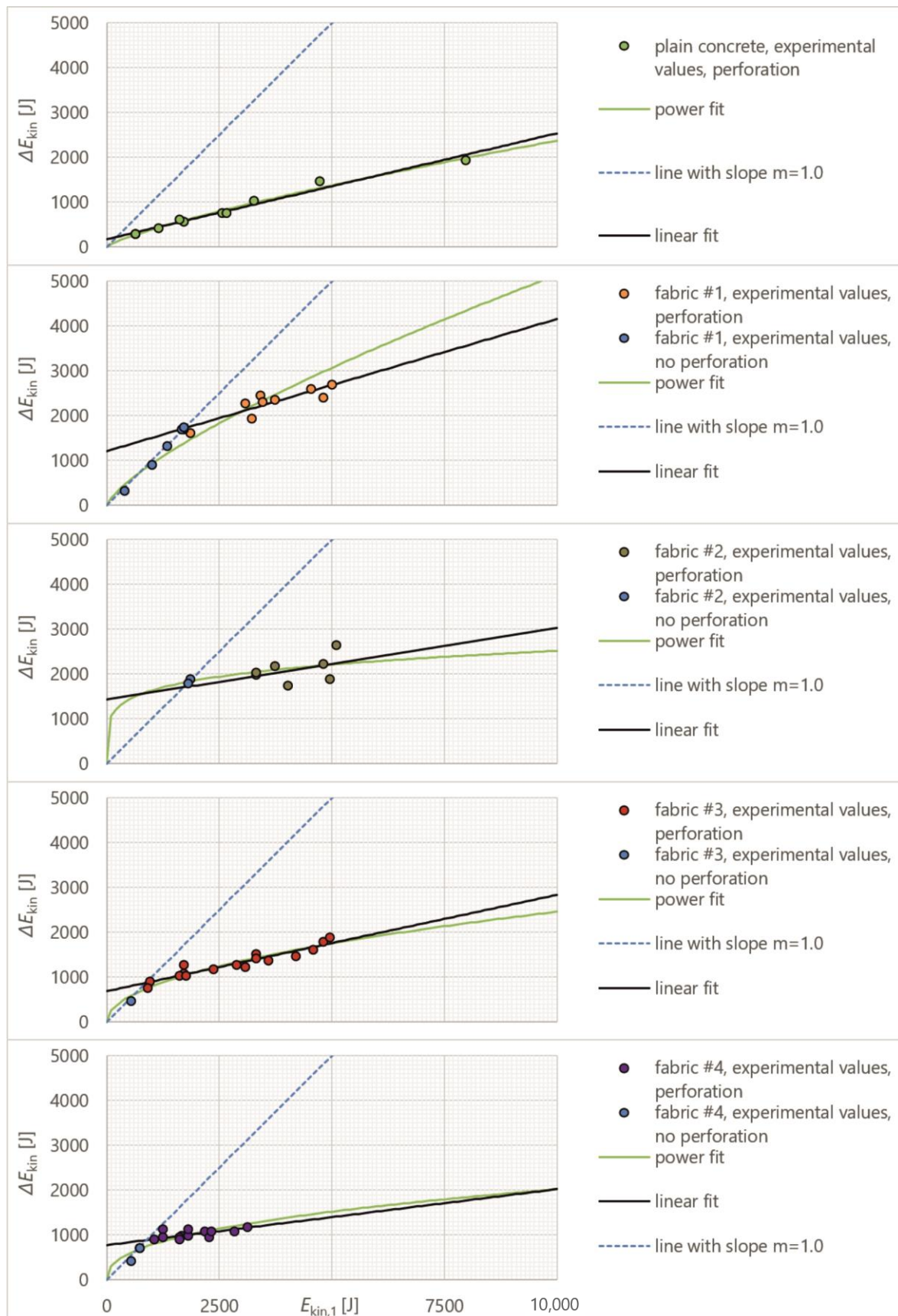


Figure 9. Visualization of the experimental results, with consideration of reinforcement and failure mode as well as linear fit.

Table 7. Linear fit parameters m and n and coefficient of determination R^2 of the experimental data.

Reinforcement Configuration	m (-)	n (J)	R^2 (-)
Plain concrete	0.236	173.6	0.9757
#1	0.295	1208.5	0.7682
#2	0.159	1428.7	0.1771
#3	0.215	688.6	0.8890
#4	0.125	774.7	0.4470

Now the fit takes account of the failure modes of the specimens as well as the experimentally determined values. It can also be noted that, unfortunately, this method still does not capture the experimental values better than the fit with a power function (Equation (3)). This can be seen from the lower coefficient of determination.

With the help of the fitted function curves, a qualitative evaluation of the experimental results is possible. However, it is difficult to draw clear conclusions from this observation as to which fabric or which fabric material is best suited for increasing the perforation resistance of the fine concrete layer. Especially at low impact energies in the range of low velocities, it is difficult to classify the sharp increase in the power function correctly. However, the perforation limits of the test specimens can be assumed to be in this range, which represents a quantitative value for the performance of the reinforcing layer.

The bilinear fit allows for the estimation of the perforation velocity described in the following section.

3.4. Estimation of Perforation Velocity Based on the Bilinear Fit

From the available experimental data and the evaluation of the experimental results so far, it is not possible to conclude a perforation velocity using the conventional statistical method. A significantly higher number of experiments with more variation in the velocity of the impactor would be necessary to reliably determine the perforation velocity.

However, it was found in the previous section that a linear fit through the experimental values that takes the failure mode into account gives a very good correlation with the experimentally determined values. Knowing that {1} all experiments with “no perforation” as a failure mode were on a straight line with the slope $m = 1.0$ and {2} all experiments with the failure mode “perforation” were also on a straight line, it was concluded that the intersection of the two straight lines can be used to determine the perforation velocity of the test specimens. The intersection point of the two straight lines is determined using Equation (5) with the conditions gathered in Equation (6). It is described using $E_{kin,1,PI}$ and $\Delta E_{kin,PI}$.

$$1.0 \cdot E_{kin,1} = m \cdot E_{kin,1} + n \quad (5)$$

$$E_{kin,1,PI} = \Delta E_{kin,1,PI} = -n/(m - 1) \quad (6)$$

If the intersection of the two straight lines is known, the perforation velocity (v_{perf}) can be calculated using Equation (1) and the known mass of the impactor (m_{Imp}); see Equation (7).

$$v_{perf} = ((2 \cdot E_{kin,1,PI})/m_{Imp})^{1/2} \quad (7)$$

Based on the perforation velocities that are compiled in Table 8, it can be seen that plates #1 and #2, reinforced with fine mesh fabrics, have significantly higher perforation velocities than plates #3 and #4, reinforced with coarse mesh fabrics. A similar observation can be made when looking at Figure 7, although the interpretation is not so clear as when taking the fit according to Equation (3) into account.

Table 8. Point of intersection and evaluated perforation velocity.

	$E_{kin,1,PI} = \Delta E_{kin,PI}(J)$	$v_{perf}(m/s)$
plain concrete	227.30	7.36
#1	1713.46	20.20
#2	1699.62	20.12
#3	876.69	14.45
#4	885.19	14.52

4. Conclusions

In this article, an extract from a test series on the resistance of thin, textile-reinforced concrete plates to an impact load was presented. The materials used, the test specimens, the test setup and the evaluation possibilities of the tests were discussed. Furthermore, based on the experimental data presented in this article, the possibility to estimate the perforation velocities of thin, textile-reinforced concrete plates was shown. A bilinear fit approach was used to calculate these velocities. With the presented evaluation method, it is possible to determine the perforation limit of thin, textile-reinforced plates with a small number of experiments. The efficiency and calculation reliability of the presented evaluation method must be verified in subsequent investigations. Thin layers of textile-reinforced concrete, i.e., mineral-bonded material composites using non-metallic reinforcement, enable existing concrete structures to be subsequently strengthened, and increase the impact resistance. In terms of sustainability, this is a valuable approach for at least two reasons. First, the non-metallic reinforcement allows for very thin and resource-saving strengthening layers. Secondly, this approach of strengthening helps to preserve existing structures and allows for an increase in service life. Preserving existing structures lengthens the life cycle of buildings and makes the demolishing and rebuilding of otherwise structurally sound buildings unnecessary. It is thus the most sustainable approach.

Author Contributions: Conceptualization, M.C., M.H. and B.B.; methodology, M.H., M.C. and J.S.; software, M.H.; validation, M.H. and M.C.; formal analysis, M.H.; investigation, M.H.; resources, M.C.; data curation, M.H.; writing—original draft preparation, M.H. and B.B.; writing—review and editing, M.C. and J.S.; visualization, M.H.; supervision, M.C. and J.S.; project administration, M.H.; funding acquisition, B.B. and M.C. All authors have read and agreed to the published version of the manuscript.

Funding: The investigations presented here represent a part of the investigations carried out in Doctoral Project A5 within the frame of the Research Training Group GRK 2250, funded by the Deutsche Forschungsgemeinschaft (German Research Foundation, DFG), project no. 287321140. Further thanks go to the research association Forschungskuratorium Textil e.V. for support in the framing of the first parametric study on the topic of the strengthening of structural components against impact loading, project no. 19009 BG/2.

Data Availability Statement: The data presented in this study are available on request from the corresponding authors. The data are not publicly available due to ongoing study.

Conflicts of Interest: The authors declare no conflict of interest. The funders had no role in the design of the study; in the collection, analyses, or interpretation of data; in the writing of the manuscript; or in the decision to publish the results.

References

1. Hering, M. Untersuchung von Mineralisch Gebundenen Verstärkungsschichten für Stahlbetonplatten Gegen Impaktbeanspruchungen (Investigation of Mineral-Bonded Strengthening Layers for Reinforced Concrete Plates against Impact loads). Ph.D. Thesis, Technische Universität Dresden, Dresden, Germany, 12 August 2020.
2. Máca, P.; Sovják, R.; Konvalinka, P. Mix design of UHPFRC and its response to projectile impact. *Int. J. Impact Eng.* **2014**, *63*, 158–163. [[CrossRef](#)]
3. Sovják, R.; Vavříník, T.; Zatloukal, J.; Máca, P.; Mičunek, T.; Frydryn, M. Resistance of slim UHPFRC targets to projectile impact using in-service bullets. *Int. J. Impact Eng.* **2015**, *76*, 166–177. [[CrossRef](#)]

4. Scheerer, S.; Zobel, R.; Müller, E.; Senckpiel-Peters, T.; Schmidt, A.; Curbach, M. Flexural Strengthening of RC Structures with TRC—Experimental Observations, Design Approach and Application. *Appl. Sci.* **2019**, *9*, 1322. [\[CrossRef\]](#)
5. Raupach, M.; Cruz, C.M. Textile-reinforced concrete: Selected case studies. In *Textile Fibre Composites in Civil Engineering*; Triantafyllou, T.C., Ed.; Woodhead Publishing: Soston, UK, 2016.
6. Erhard, E.; Weiland, S.; Lorenz, E.; Schladitz, F.; Beckmann, B.; Curbach, M. Anwendungsbeispiele für Textilbetonverstärkung—Instandsetzung und Verstärkung bestehender Tragwerke mit Textilbeton. *Beton Stahlbetonbau* **2015**, *110*, 74–82. [\[CrossRef\]](#)
7. Hering, M.; Curbach, M. A new testing method for textile reinforced concrete under impact load. In *Web of Conferences, Proceedings of the ICCRRR: 5th International Conference on Concrete Repair, Rehabilitation and Retrofitting, Cape Town, South Africa, 19–21 November 2018*; Alexander, M.G., Beushausen, H., Dehn, F., Moyo, P., Eds.; EDP Sciences: Ulis, France, 2018.
8. Hering, M.; Kühn, T.; Curbach, M. Small-scale plate tests with fine concrete in experiment and first simplified simulation. *Struct. Concr.* **2020**, *22*, 637–649. [\[CrossRef\]](#)
9. Tahenti, B.; Coghe, F.; Nasri, R. Ballistic Limit Estimation Approaches for Ballistic Resistance Assessment. *Def. Sci. J.* **2020**, *70*, 82–89. [\[CrossRef\]](#)
10. Johnson, T.H.; Freeman, L.; Hester, J.; Bell, J.L. A Comparison of Ballistic Resistance Testing Techniques in the Department of Defense. *IEEE Access* **2014**, *2*, 1442–1455. [\[CrossRef\]](#)
11. Kneubuehl, B.P. *Ballistic Protection*; bpk consultancy GmbH: Thun, Switzerland, 2002.
12. PAGEL®Spezial-Beton GmbH & Co. KG: TEXTILFEINBETON. Technisches Merkblatt 0606/QS-Formblatt 10/21 Rev. 06. Available online: https://www.pagel.com/all/pdf/de/tf10_de.pdf (accessed on 27 April 2022).
13. DIN EN 196-1; Prüfverfahren für Zement—Teil 1: Bestimmung der Festigkeit; Deutsche Fassung EN 196-1:2016—Methods of Testing Cement—Part 1: Determination of Strength; German Version EN 196-1:2016. European Standards: Prague, Czech Republic, 2016.
14. Valmieras Stikla Škiedra. *Technisches Datenblatt S 55–SSA–1363–14SM*; Version Nr. 4, 31.03.2010; Valmieras Stikla Škiedra: Riga, Latvia, 2010.
15. Lorenz, E. Endverankerung und Übergreifung Textiler Bewehrungen in Betonmatrices (End Anchorage and Overlapping of Textile Reinforcements in Concrete). Ph.D. Thesis, Technische Universität Dresden, Dresden, Germany, 16 December 2014.
16. Schütze, E.; Bielak, J.; Scheerer, S.; Hegger, J.; Curbach, M. Einaxialer Zugversuch für Carbonbeton mit textiler Bewehrung | Uniaxial tensile test for carbon reinforced concrete with textile reinforcement. *Beton Stahlbetonbau* **2018**, *113*, 33–47. [\[CrossRef\]](#)
17. Schütze, E.; Curbach, M. Zur experimentellen Charakterisierung des Verbundverhaltens von Carbonbeton mit Spalten als maßgeblichem Versagensmechanismus. *Bauingenieur* **2019**, *94*, 133–141. [\[CrossRef\]](#)
18. Cherif, C.; Zierold, K.; Curbach, M.; Hering, M. *Schlussbericht zu IGF-Vorhaben Nr. 19009 BG Textilverstärkte Betonkonstruktionen für Impaktbeanspruchungen (Impakt-Textilbeton-Konstruktionen)*; Technische Universität Dresden: Dresden, Germany, 2019.
19. DIBT. *Allgemeine Bauaufsichtliche Zulassung: Verfahren zur Verstärkung von Stahlbeton mit TUDALIT (Textilbewehrter Beton)*, Zulassungsnummer Z-31.10-182, Geltungsdauer: Vom 1.6. 2015—1.6. 2016; Deutsches Institut für Bautechnik: Berlin, Germany, 2016.
20. Solidian GmbH. *Technisches Datenblatt/Technical Data Sheet Solidian GRID Q142/142-CCE-38, Version 171129*, 29.11.2017; Solidian GmbH: Albstadt, Germany, 2017.
21. Solidian GmbH. *Technisches Datenblatt/Technical Data Sheet Solidian GRID Q85/85-CCE-21, Version 190423*, 23.04.2019; Solidian GmbH: Albstadt, Germany, 2019.
22. Just, M.; Curbach, M.; Hering, M. *Bauteilverhalten Unter Stoßartiger Beanspruchung Durch Aufprallende Behälter (Flugzeugtanks); Phase 1A: Maßstabeffekte bei Stoßartiger Beanspruchung. Abschlussbericht zum Reaktorsicherheitsforschungs-Vorhaben Nr. 1501438, Gefördert Durch das Bundesministerium für Wirtschaft und Energie (BMWi); Institut für Massivbau der TU Dresden: Hannover, Germany, 2016; 208p.*
23. Hering, M.; Kühn, T.; Curbach, M. *Bauteilverhalten Unter Stoßartiger Beanspruchung Durch Aufprallende Behälter (Flugzeugtanks); Phase 1B: Quantifizierung der Schädigungen des Betongefüges, Teilprojekt: Fallturmversuche. Abschlussbericht zum Reaktorsicherheitsforschungs-Vorhaben Nr. 1501479, Gefördert Durch das Bundesministerium für Wirtschaft und Energie (BMWi); Institut für Massivbau der TU Dresden: Hannover, Germany, 2017; 415p.*

Disclaimer/Publisher's Note: The statements, opinions and data contained in all publications are solely those of the individual author(s) and contributor(s) and not of MDPI and/or the editor(s). MDPI and/or the editor(s) disclaim responsibility for any injury to people or property resulting from any ideas, methods, instructions or products referred to in the content.